Optics Communications 282 (2009) 459–464

Contents lists available at ScienceDirect

Optics Communications

journal homepage: www.elsevier.com/locate/optcom

Sharply focusing a radially polarized laser beam using a gradient Mikaelian's microlens

V.V. Kotlyar, S.S. Stafeev *

Image Processing Systems Institute of the Russian Academy of Sciences, S.P. Korolyev Samara State Aerospace University, Molodogvardeiskaya, 151, Samara 443001, Russia

ARTICLE INFO

Article history:
Received 5 May 2008
Received in revised form 15 October 2008
Accepted 30 October 2008

Keywords:
Radial FDTD method
Sharp focusing of light
Gradient Mikaelian's microlens
Minimal focal spot size

ABSTRACT

Focusing a radially polarized annular Gaussian beam with a gradient Mikaelian's microlens is simulated using a radial version of the FDTD method (finite-difference time domain), in which Maxwell's equations in the cylindrical coordinates are solved in the MATLAB 7.0 environment. We show that the focal spot size (the area with larger-than half-maximum intensity) can be made as small as $0.126\lambda^2$, with focal spot diameter being 0.40λ.

1. Introduction

In the recent years, great interest has been expressed in sharp focusing of laser light and reaching a minimal focal spot size beyond the diffraction limits. Decreasing the focal spot size is critical in lithography, optical memory and micromanipulation. For example, in a recent paper [1] it was shown that radially polarized sharp laser beams could be used to accelerate protons and carbon nuclei in medical applications. In Ref. [2] (see also the list of references in [2]) the application of focused laser beams in optical microscopy and optical coherent tomography was discussed. The radially polarized laser beams can easily be generated using, for example, interferometers [3] or a segmented half-wave plate [4,5].

Recently, record-breaking results in sharp focusing have been reported. In Ref. [5] a microobjective Leika plan, apo 100×, of numerical aperture NA = 0.9, was used to focus in air a radially polarized laser beam into a spot size of half-maximum intensity (where the intensity exceeds its half-maximum, half-maximum area, HMA) equal to HMA = $0.16\lambda^2$ and with spot diameter (Full Width at Half-Maximum, FWHM) FWHM = 0.451λ, where λ is the wavelength in free space. The experiment used a fundamental He–Ne laser mode of wavelength 632.8 nm, with an annular mask obstructing the central part (3 mm in diameter) of the 3.6-mm incident beam. In more recent publications [6], still better result was reported. In Ref. [6], a parabolic mirror (19 mm in diameter and NA = 0.999) was utilized to experimentally focus a radially polarized laser beam of wavelength 632.8 nm into a focal spot of HMA = $0.134\lambda^2$. The intensity distribution in the focal plane was measured using a 40-nm fluorescent bead. The focal spot diameter was reported to be 0.45λ. Note that this value can be reduced still further, since the numerical simulation based on Debye's theory and Richards–Wolf's equations showed [7] that using a conventional diffraction lens or a parabolic mirror of NA = 0.98, the radially polarized hollow Gaussian beam of amplitude $r\exp(-r^2/w^2)$ (r is the radial coordinate and w is the Gaussian beam waist radius) could be focused into a spot of HMA = $0.210\lambda^2$ or HMA = $0.157\lambda^2$, respectively. For a parabolic mirror of NA = 1 the calculations conducted in Ref. [7] showed that the focal spot size can be further reduced to a value less than HMA = $0.154\lambda^2$. If the Gaussian beam is bounded by a narrow annular diaphragm (resulting in a partial loss of the light energy), then the focal spot size can be decreased to HMA = $0.101\lambda^2$. By comparison, in the paraxial scalar approximation, the focal spot size for the Airy disk is HMA = $0.204\lambda^2$.

In this paper, we numerically simulate focusing a radially polarized annular Gaussian beam $\exp(-(r-r_0)^2/w^2)$ with a cylindrical Mikaelian's microlens of diameter 12 μm and thickness 10 μm. We show that the focal spot size (the area with larger-than half-maximum intensity) is equal to HMA = $0.126\lambda^2$. Compared with the results reported in Refs. [5–7], this is the best result, to the best of our knowledge, obtained so far by means of refractive optics.

1.1. The radial FDTD method

For the rigorous calculation of light diffraction by axially symmetric optical elements, Prather and Shi [8] proposed an FDTD-method version, which solved Maxwell's equations in the cylindrical coordinates. However, the diffraction of the radially polarized

* Corresponding author.
E-mail address: sergej_ss_2004@mail.ru (S.S. Stafeev).

0030-4018/$ - see front matter © 2008 Elsevier B.V. All rights reserved.
doi:10.1016/j.optcom.2008.10.057

light was not discussed in Ref. [8]. In this section, we discuss an FDTD-method version specially designed to calculate the diffraction of a radially polarized laser beam by axially symmetric microoptics elements. For the radially polarized incident beam, the electric field vector is directed along the radial coordinate in a cylindrical coordinate system. Let a monochromatic radially polarized electromagnetic wave propagating along the optical axis z is incident normally onto an axially symmetric refractive optical element. To derive the wave propagation equation, Maxwell's equations can be expressed in the cylindrical coordinates (r, ϕ, z) as follows:

$$\frac{1}{r}\frac{\partial H_z}{\partial \phi} - \frac{\partial H_\phi}{\partial z} = \varepsilon\varepsilon_0 \frac{\partial E_r}{\partial t} \tag{1}$$

$$\frac{\partial H_r}{\partial z} - \frac{\partial H_z}{\partial r} = \varepsilon\varepsilon_0 \frac{\partial E_\phi}{\partial t} \tag{2}$$

$$\frac{1}{r}\frac{\partial (rH_\phi)}{\partial r} - \frac{1}{r}\frac{\partial H_r}{\partial \phi} = \varepsilon\varepsilon_0 \frac{\partial E_z}{\partial t} \tag{3}$$

$$\frac{1}{r}\frac{\partial E_z}{\partial \phi} - \frac{\partial E_\phi}{\partial z} = -\mu\mu_0 \frac{\partial H_r}{\partial t} \tag{4}$$

$$\frac{\partial E_r}{\partial z} - \frac{\partial E_z}{\partial r} = -\mu\mu_0 \frac{\partial H_\phi}{\partial t} \tag{5}$$

$$\frac{1}{r}\frac{\partial (rE_\phi)}{\partial r} - \frac{1}{r}\frac{\partial E_r}{\partial \phi} = -\mu\mu_0 \frac{\partial H_z}{\partial t} \tag{6}$$

where E_γ, H_γ are the electric and magnetic field strengths, respectively ($\gamma = r, z, \phi$ are the axial components) and r is the distance to the symmetry axis.

All the components are expanded into the Fourier series in terms of the polar angle ϕ as

$$E_\gamma(r,z,\phi,t) = \frac{E_{\gamma 0}(r,z,t)}{2} + \sum_{k=1}^{\infty} E^{(1)}_{\gamma,k}(r,z,t)\cos(k\phi) + E^{(2)}_{\gamma,k}(r,z,t)\sin(k\phi) \tag{7}$$

$$H_\gamma(r,z,\phi,t) = \frac{H_{\gamma 0}(r,z,t)}{2} + \sum_{k=1}^{\infty} H^{(1)}_{\gamma,k}(r,z,t)\cos(k\phi) + H^{(2)}_{\gamma,k}(r,z,t)\sin(k\phi) \tag{8}$$

The amplitudes of the electric and magnetic fields in Eqs. (7) and (8) are independent of the polar angle ϕ.

For a radially polarized monochromatic plane wave, propagating along optical axis z, we can write $E^{inc} \equiv E^{inc}_r = \cos\omega t$, where ω is the circular light frequency. In this case, only three components of the electromagnetic field (7) and (8) are non-zero: $E_{r,0}$, $E_{z,0}$, $H\phi_{,0}$. These are the radial and longitudinal components of the electric field and the azimuthal component of the magnetic field. The zero index means that all three components are independent on the azimuthal angle ϕ. Therefore, six Maxwell's equations. (1)–(6) for radially polarized light reduce to three equations:

$$-\frac{\partial H_{\varphi,0}}{\partial z} = \varepsilon\varepsilon_0 \frac{\partial E_{r,0}}{\partial t} + \sigma E_{r,0}, \tag{9}$$

$$\frac{1}{r}\frac{\partial (rH_{\varphi,0})}{\partial r} = \varepsilon\varepsilon_0 \frac{\partial E_{z,0}}{\partial t} + \sigma E_{z,0}, \tag{10}$$

$$\frac{\partial E_{r,0}}{\partial z} - \frac{\partial E_{z,0}}{\partial r} = -\mu\mu_0 \frac{\partial H_{\varphi,0}}{\partial t}, \tag{11}$$

where ε and μ are the relative electric and magnetic permeabilities of the optical element material (further, $\mu = 1$), ε_0 and μ_0 are the electric and magnetic permeabilities of vacuum, σ is the relative conductivity (further, $\sigma = 0$). Conditionally stable, explicit difference equations that approximate Eqs. (9) and (10) are given by

$$\varepsilon\left(i+\frac{1}{2},j\right)\varepsilon_0 \frac{E^n_{r,0}(i+\frac{1}{2},j) - E^{n-1}_{r,0}(i+\frac{1}{2},j)}{\Delta t} = -\frac{H^{n-\frac{1}{2}}_{\phi,0}(i+\frac{1}{2},j+\frac{1}{2}) - H^{n-\frac{1}{2}}_{\phi,0}(i+\frac{1}{2},j-\frac{1}{2})}{\Delta z} \tag{12}$$

$$\varepsilon\left(i,j+\frac{1}{2}\right)\varepsilon_0 \frac{E^n_{z,0}(i,j+\frac{1}{2}) - E^{n-1}_{z,0}(i,j+\frac{1}{2})}{\Delta t} = \frac{1}{r(i)}\frac{r(i+\frac{1}{2})H^{n-\frac{1}{2}}_{\phi,0}(i+\frac{1}{2},j+\frac{1}{2}) - r(i-\frac{1}{2})H^{n-\frac{1}{2}}_{\phi,0}(i-\frac{1}{2},j+\frac{1}{2})}{\Delta r} \tag{13}$$

$$-\mu_0 \frac{H^{n+\frac{1}{2}}_{\phi,0}(i+\frac{1}{2},j+\frac{1}{2}) - H^{n-\frac{1}{2}}_{\phi,0}(i+\frac{1}{2},j+\frac{1}{2})}{\Delta t} = \frac{E^n_{r,0}(i+\frac{1}{2},j+1) - E^n_{r,0}(i+\frac{1}{2},j)}{\Delta z} - \frac{E^n_{z,0}(i+1,j+\frac{1}{2}) - E^n_{z,0}(i,j+\frac{1}{2})}{\Delta r} \tag{14}$$

where Δt, Δr, Δz are the sampling steps for the corresponding axes; n, i, j are the integer indices of nodes in the coordinate grid t, r, z. The time step Δt must satisfy the condition [8]

$$c\Delta t \le \frac{\min(\Delta r, \Delta z)}{\sqrt{2}}, \tag{15}$$

where c is the speed of light in vacuum. The radiation was coupled into the computation domain using a hard source model. To these ends, the E_r component was assumed to change in time as

$$E^n_{r,0}(i,j) = E_0(i,j)\sin(\omega\Delta t n). \tag{16}$$

In the difference equations (12)–(14) we used Yee grid with half-integer steps [9]. The boundary conditions were chosen in the form of a perfectly matched layer [10]. Peculiarities of calculating the field on the optical axis ($r = 0$) can be found in Ref. [8].

2. Simulation results

Using Eqs. (12)–(14), we simulated focusing the radially polarized Gaussian beam propagating along the optical axis and incident onto a gradient Mikaelian's microlens with cylindrical symmetry. The refractive index in the gradient lens changes as a secant [11]:

$$n(r) = n_0\left[ch\left(\frac{\pi r}{2L}\right)\right]^{-1} \tag{17}$$

where n_0 is the refractive index on the axis and L is the lens axial thickness. The lens radius R is derived from Eq. (17), considering that $n(R) = 1$.

Fig. 1 shows the radial section of the Mikaelian's microlens ($n_0 = 1.5$): the radius along the radial axis is $R = 6$ μm, the thickness along the optical axis (vertical axis in Fig. 1) is $L = 10$ μm. The calculation domain size is 20 μm × 8 μm, the sampling step of $\lambda/50$ is

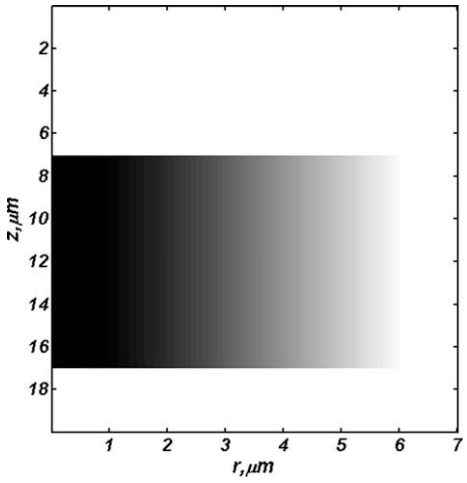

Fig. 1. Size of the gradient axially symmetric Mikaelian's microlens.

the same for the r- and z-axes, and for the time axis, t is $\pi/50\omega$ (see Eq. (15)). The operating wavelength is $\lambda = 1$ μm.

Fig. 2 shows a plausible optical setup to focus the laser light using a microlens. The linearly polarized fundamental mode of laser L (Gaussian beam) passes through interferometer I (or a segmented half-wave plate), becoming radially polarized, and is then imaged with spherical lens SL. Note that a microlens ML is placed in the imaging plane of Gaussian beam (Fig. 1). ML is fabricated in a glass substrate using, for example, e-beam lithography and ion-beam etching. To image the radially polarized Gaussian beam of radius $w_0 = 1$ mm (at the output of interferometer I) as a Gaussian beam of radius $w = 7$ μm in the plane of microlens ML,

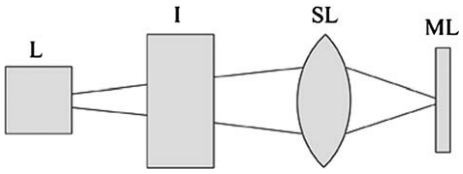

Fig. 2. Optical setup to focus the radially symmetric Gaussian beam with a microlens.

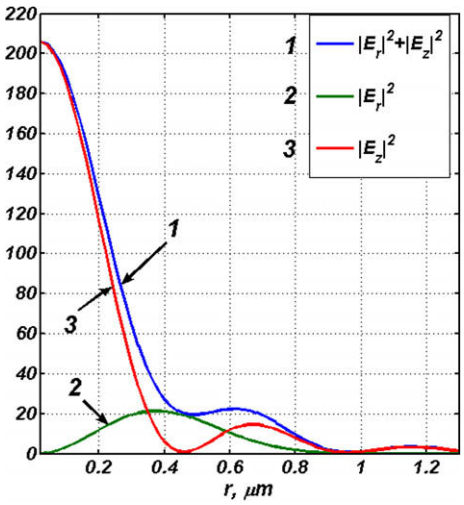

Fig. 4. Radial intensity distribution in the focal plane (immediately behind the lens surface, $z = 7$ μm) of the gradient Mikaelian's microlens illuminated by the radially polarized Gaussian beam: $|E_r|^2 + |E_z|^2$ (curve 1); $|E_r|^2$ (curve 2); $|E_z|^2$ (curve 3).

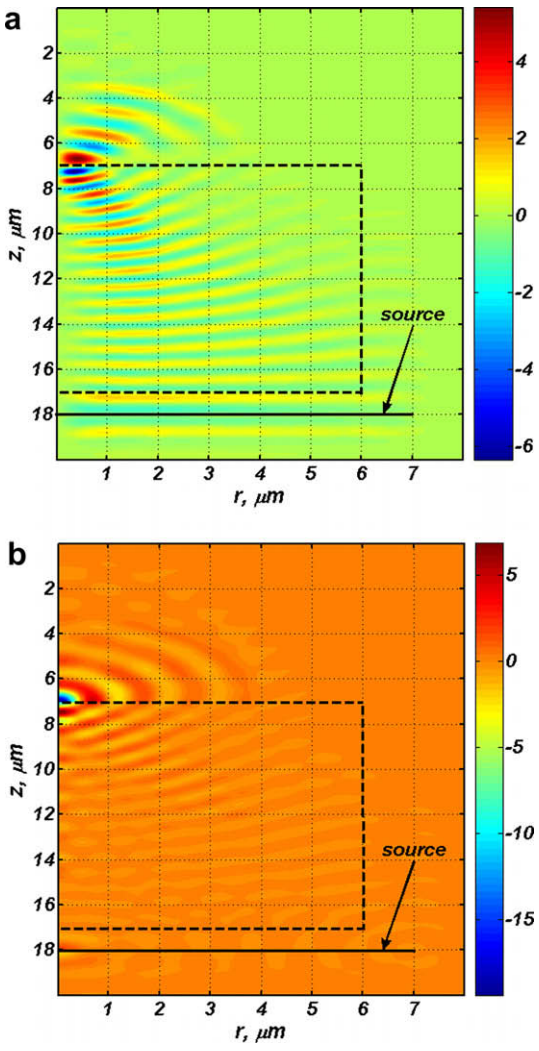

Fig. 3. Snapshot distributions of the amplitude E_r (a) and E_z (b) for diffraction of the radially polarized Gaussian beam by the gradient Mikaelian's microlens (the lens base is placed between 7 μm and 17 μm on the vertical axis).

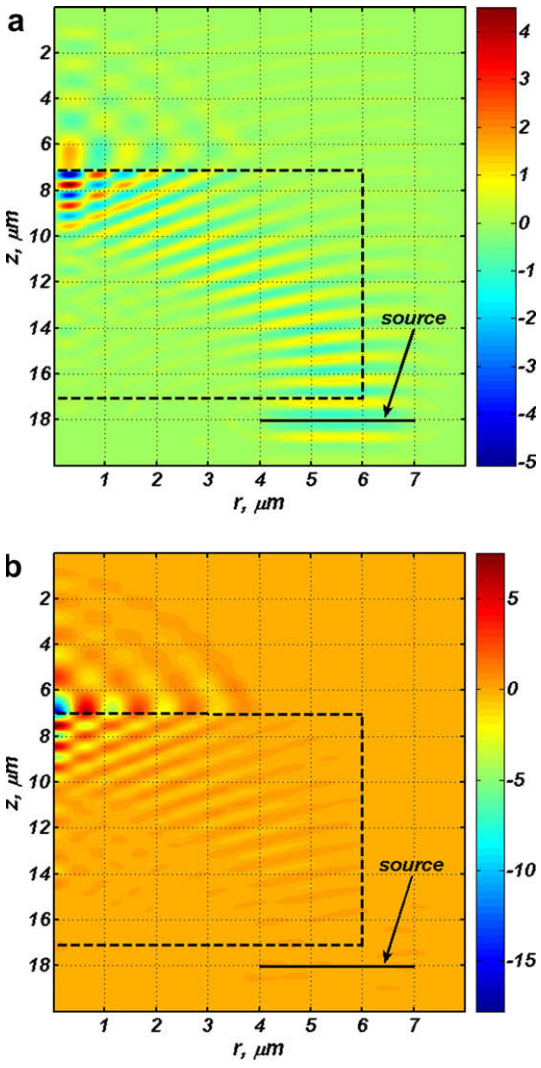

Fig. 5. Snapshot distributions of the amplitude E_r (a) and E_z (b) for diffraction of the radially polarized annular Gaussian beam (black line: the beam waist) by the gradient Mikaelian's microlens.

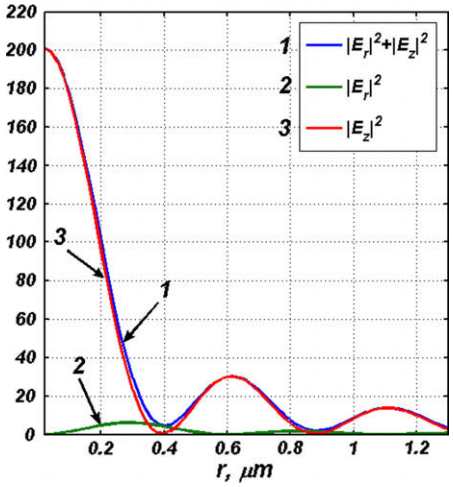

Fig. 6. Radial intensity distributions in the focal plane (immediately behind the lens surface, $z = 7$ μm) of the gradient Mikaelian's microlens illuminated by the radially polarized annular Gaussian beam: $|E_r|^2 + |E_z|^2$ (curve 1); $|E_r|^2$ (curve 2); $|E_z|^2$ (curve 3).

we can make use a lens SL of focus $f = 10$ mm. Then, the image is formed at the distance z_2 [12]:

$$z_2 = f + \frac{(z_1 - f)f^2}{(z_1 - f)^2 + z_0^2} \tag{18}$$

where $z_0 = kw_0^2/2$ is a Rayleigh distance, z_1 is a distance from Gaussian beam with w_0 to SL. In our case: $z_0 = 3145$ mm ($\lambda = 1$ μm), $z_1 = 1430$ mm and $z_2 = 10.02$ mm.

Fig. 3 shows snapshot diffraction patterns of the amplitude distribution E_r (a)and E_z (b) of the Gaussian beam $E_{r,0} = \exp(-r^2/w^2)$ of waist radius $w = 7$ μm propagating along the optical axis. In Fig. 3, a horizontal line with the "source" caption depicts the waist plane of the Gaussian beam incident on the microlens. The microlens position is indicated as a dotted line. Fig. 4 shows (in relative units) the radial distribution of the intensity: $|E_r|^2 + |E_z|^2$ (curve 1), $|E_r|^2$ (curve 2), and $|E_z|^2$ (curve 3) in the focal plane (immediately behind the lens surface, $z = 7$ μm). The focal spot diameter is FWHM = 0.48λ and the size is HMA = $0.181\lambda^2$. Let us compare the focal spot under discussion with the focal spot of the Airy disk, which is described by the Bessel function of the first order, $2J_1(x)/x$. At the half-maximum intensity, the width of the Airy disk is FWHM = 0.51λ/NA. The minimal size of the Airy disk is achieved when the numerical aperture is maximal, NA = 1, amounting to HMA = $0.204\lambda^2$. Thus, for a gradient microlens (Fig. 1) the size of the focal spot (Fig. 4, curve 1) is smaller than the diffraction limit of resolution. Note that the numerical aperture of the gradient

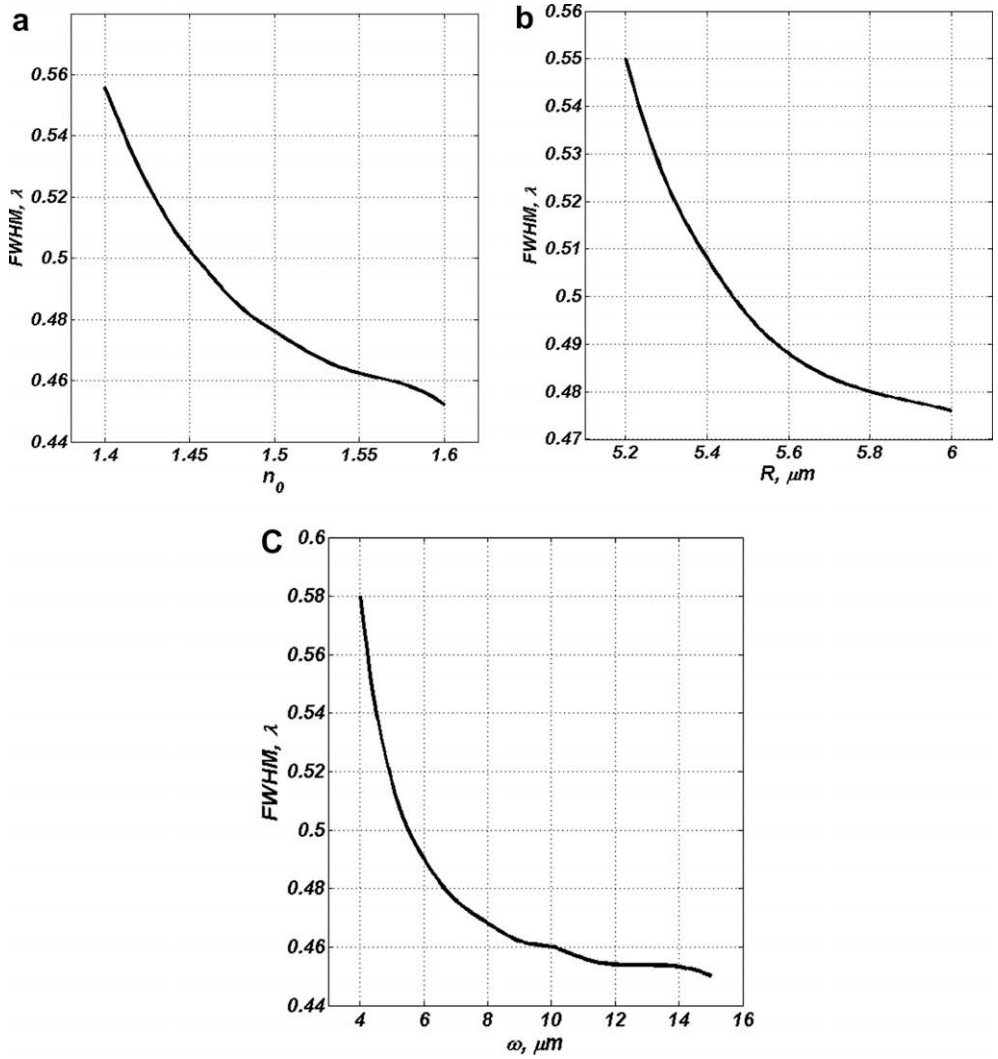

Fig. 7. The FWHM (in terms of wavelengths (λ)) of the focal spot as a function of: (a) the refractive index on the axis n_0; (b)the microlens radius R; and (c) the radius w of the illuminating beam. The rest simulation parameters are the same as in Fig. 3.

microlens (Fig. 1) can be assessed using the relation NA = $R/(L^2+R^2)^{1/2}$ = 0.514. The focal spot of a conventional refractive lens with such a NA will be twice as large as the minimal size of the Airy disk (FWHM = 0.51λ). It can also be seen from Fig. 4 that the full intensity $|E_r|^2 + |E_z|^2$ in the focal spot is practically equal to the intensity of the axial electric component $|E_z|^2$, whereas the intensity of the radial component $|E_r|^2$ amounts to 10% of the maximum of the full intensity.

To further improve this result (Fig. 4), we illuminated the microlens (Fig. 1) by the annular Gaussian beam exp $(-(r-r_0)^2/w^2)$, where r_0 = 5.5 μm and w = 1.5 μm. In Fig. 5 we show the snapshot patterns of the amplitude distributions E_r (a) and E_z (b) for this case. The black horizontal line is the source of the annular Gaussian beam. The location of the lens is indicated with a dotted line. Fig. 6 shows the radial intensity distributions $|E_r|^2 + |E_z|^2$ (curve 1), $|E_r|^2$ (curve 2) and $|E_z|^2$ (curve 3) in the focal plane. The focal spot diameter is FWHM = 0.40λ, and the size is HMA = 0.126λ^2. Fig. 6 suggests that the curve of full intensity $|E_r|^2 + |E_z|^2$ nearly coincides with that of the axial field component $|E_z|^2$, while the maximal value of the radial component $|E_r|^2$ amounts to less than 5% of the maximal value of full intensity.

The focal spot size (compare Fig. 6 and Fig. 4) is decreased by 1.44 and the diameter by 1.2, but the intensity in the focus is also decreased (by 1.06) and the lateral intensity is increased (by 1.3). The focal spot shown in Fig. 6 has a smaller size as compared with the focal spot size in Refs. [5–7].

Note that attempts to realize an exact annular Gaussian beam defined by exp $(-(r-r_0)^2/w^2)$ have failed. In practice, however, there are several alternatives. A thin metallic film with an annular diaphragm can be preliminary sprayed onto a microlens bulk substrate. The modeling we conducted has shown that when focusing a Gaussian beam of waist radius 7 μm bounded by a circular diaphragm of radii R_1 = 4 μm and R_2 = 7 μm, the FWHM of the resulting focal spot will be almost the same as that in Figs. 5 and 6, with the maximal intensity being two times smaller. An annular laser beam can also be experimentally generated with a conical axicon placed between the lens SL and the microscope ML in the optical configuration of Fig. 2. Another technique for generating the annular Gaussian beam was presented in Ref. [7]. In this work, the modeling was conducted using a beam r exp$(-r^2/w^2)$, which can be generated with an amplitude mask whose transmittance is changing linearly with radius from zero to unity. In Ref. [13], the sharp focusing was modeled using an annular Bessel–Gauss beam in the form $J_1(2r)$ exp$(-r^2)$.

Such a beam cannot be implemented with an amplitude mask because the Bessel function can take both positive and negative values.

Fig. 7a shows the FWHM of the focal spot as a function of the refractive index n_0 on the lens optical axis in Eq. (17), the rest simulation parameters being the same as in Figs. 3 and 4. Note that the lens radius was also changed to satisfy the condition $n(R)$ = 1. Hence it is seen that with increasing n_0 the FWHM of the focal spot is decreasing. From Fig. 7a it also follows that the focal spot becomes smaller than the diffraction limit (of the Airy disk, FWHM = 0.51λ) at n_0 > 1.45. Fig. 7b shows the FWHM as a function of lens radius R at a fixed refractive index on the axis, n_0 = 1.5, the rest simulation parameters being the same as in Fig. 3. From Fig. 7b it follows that with increasing lens radius, the focal spot diameter is decreasing, so that the diffraction limit can be overcome at R > 5.4 μm. Note that the refractive index of the lens at the edge is n(5.4) = 1.08. Fig. 7c shows the FWHM in terms of wavelengths versus the Gaussian beam radius w (the rest simulation parameters being the same as in Fig. 3). Fig. 7c suggests that the focal spot becomes smaller than the diffraction limit at w>5.5 μm. It is noteworthy that if the Gaussian beam radius is being further increased, becoming larger than the lens radius (w > 6 μm), the focal spot diameter continues to decrease. This decrease occurs until the min-

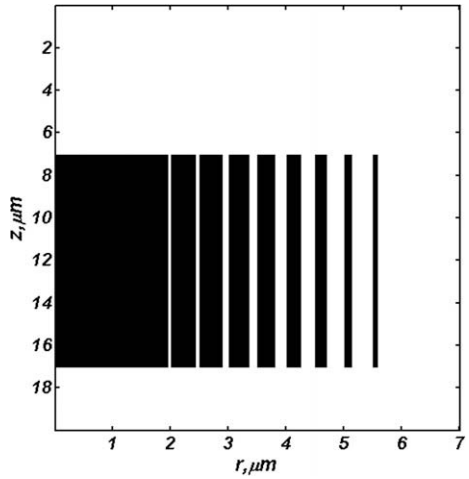

Fig. 8. A binary Mikaelian's lens as a plausible replacement of the gradient lens in Fig. 1.

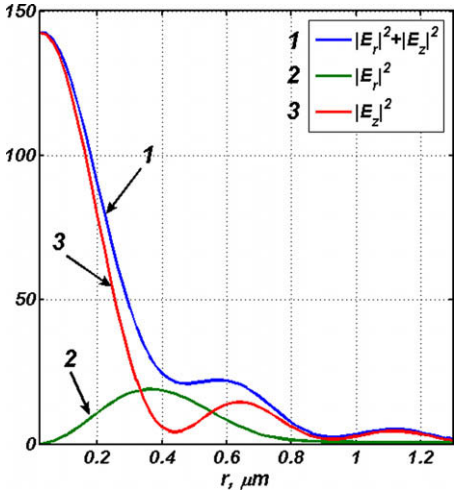

Fig. 9. Radial intensity distributions in the focal plane (immediately behind the lens surface, z = 7 μm) of the binary Mikaelian's microlens (Fig. 8) illuminated by the radially polarized Gaussian beam: $|E_r|^2 + |E_z|^2$ (curve 1); $|E_r|^2$ (curve 2); $|E_z|^2$ (curve 3).

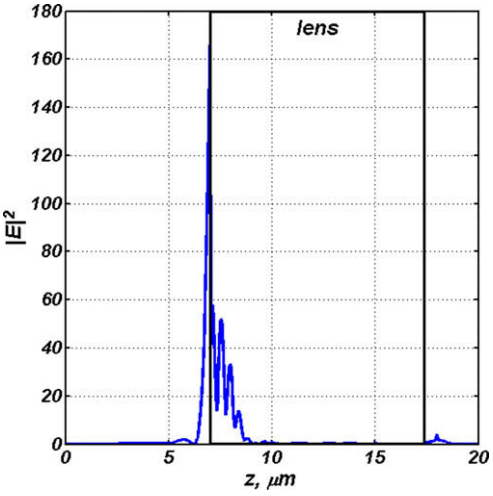

Fig. 10. Full intensity $|E_r|^2 + |E_z|^2$ on the optical axis for the binary lens of Fig. 8. The simulation parameters are the same as in Fig. 9.

imal value of the FWHM = 0.45λ is reached at the Gaussian beam radius of w = 15 μm. Further increase in the Gaussian beam radius (the lens parameters are constant) does not result in the decrease of the focal spot size.

The gradient microlens can be realized as a photonic crystal lens using microlithography technology [14]. A binary version of the gradient lens with cylindrical symmetry represents a fragment of Bragg's optical fiber (Fig. 8) [15]. Fig. 8 shows a binary Mikaelian's lens with e same geometric parameters as in Fig. 1. Within each discretization step Δr = 0.5 μm, the width $x(r)$ of the lens material along the radial coordinate r was chosen from the condition

$$x(r) = \Delta r\left[\frac{n(r)-1}{n_0-1}\right] \tag{19}$$

where n_0 and $n(r)$ were taken from Eq. (17). Fig. 9 shows (in relative units) the radial distributions of the intensity: $|E_r|^2 + |E_z|^2$ (curve 1), $|E_r|^2$ (curve 2) and $|E_z|^2$ (curve 3) in the focal plane (immediately behind the binary lens plane in Fig. 8) when the lens is illuminated by a radially polarized Gaussian beam of radius w = 7 μm and wavelength λ = 1 μm. The refractive index of the binary lens material in Fig. 8 is n = 1.5. From Fig. 9 it is seen that when the gradient lens (Fig. 1) is replaced with a binary lens (Fig. 8) the maximal intensity of the focal spot is insignificantly decreased (by 20%), whereas the focal spot size remains practically unchanged (nearly the same as in Fig. 4). Fig. 10 shows the longitudinal axial distribution of the full intensity $|E_r|^2 + |E_z|^2$ for the binary lens (Fig. 8). From Fig. 10, it is seen that the depth of focus (distance between the adjacent local intensity minima along the optical axis) approximately equals the wavelength, with the intensity maximum attained just behind the lens plane (the location of the lens is shown in Fig. 10).

3. Conclusions

In this study, we have obtained the following results:

- We have considered a radial variant of the FDTD-method designed for solving Maxwell's equations in the cylindrical coordinates for radially polarized light, realizing it in the MATLAB 7.0 environment.
- Focusing the radially polarized annular Gaussian beam with a gradient Mikaelian's microlens has been simulated and it has been shown that the focal spot size (the area with larger-than half-maximum intensity) can be reduced to $0.126\lambda^2$, with the spot diameter being 0.40λ. These results surpass those reported in Refs. [5,6].

Acknowledgments

This work was financially supported by the Russian–American program "Basic Research and Higher Education" (CRDF Grant # RUX0-014-SA-06), the Russian Foundation for Basic Research (Grant # 08-07-99007) and the Russian Federation Presidential Grant NSH-3086.2008.9.

References

[1] Y.I. Salamin, Z. Harman, C.H. Keitel, Phys. Rev. Lett. 100 (2008) 155004.
[2] L. Lin, F. Diaz, L. Wang, B. Lioseaux, J. Huignard, C.J.R. Sheppard, N. Chen, J. Opt. Soc. Am. A 25 (8) (2008) 2095.
[3] S.C. Tidwell, D.H. Ford, W.D. Kimura, Appl. Opt. 29 (15) (1990) 2234.
[4] H. Kawauchi, Y. Kozava, S. Sato, T. Sato, S. Kawakami, Opt. Lett. 33 (4) (2008) 399.
[5] R. Dorn, S. Quabis, G. Leuchs, Phys. Rev. Lett. 91 (2003) 233901.
[6] J. Stadler, C. Stanciu, C. Stupperich, A.J. Meixner, Opt. Lett. 33 (7) (2008) 681.
[7] N. Davidson, N. Bokor, Opt. Lett. 29 (12) (2004) 1318.
[8] D.W. Prather, S. Shi, J. Opt. Soc. Am. A 16 (5) (1999) 1131.
[9] K.S. Yee, IEEE Trans. Anten. Prop. AP-14 (1966) 302.
[10] J.P. Berenger, Comput. Phys. 114 (1994) 185.
[11] A.L. Mikaelian, Doklady USSR Acad. Sci. (81) (1951) 569.
[12] H. Kogelnik, Bell. Syst. Tech. J. 44 (3) (1965) 455.
[13] V.P. Kalosha, I. Golub, Opt. Lett. 32 (24) (2007) 3540.
[14] Y.R. Triandaphilov, V.V. Kotlyar, Opt. Mem. Neur. Net. (Inform. Opt.) 17 (1) (2008) 1.
[15] M. Skorobogatiy, N. Guo, Opt. Lett. 32 (8) (2007) 900.